International Journal of Automotive Technology, Vol. 16, No. 1, pp. 39–49 (2015)
DOI 10.1007/s12239–015–0004–7

pISSN 1229–9138/ eISSN 1976–3832

FINITE ELEMENT BASED IMPROVEMENT OF A LIGHT TRUCK DESIGN TO OPTIMIZE CRASHWORTHINESS

D. Y. CHEN[1)], L. M. WANG[1)*], C. Z. WANG[2)], L. K. YUAN[3)], T. Y. ZHANG[3)] and Z. Z. ZHANG[3)]

[1)]School of Mechanical Engineering, Nanjing University of Science & Technology, Nanjing 210094, China
[2)]Department of Mechanical Engineering and Materials Science, University of Pittsburgh, Pittsburgh, Pennsylvania 15261, USA
[3)]Product Engineering, Nanjing Iveco Automobile Co., Ltd., 100 Heimoying, Nanjing 210028, China

(Received 7 June 2013; Revised 10 October 2013; Accepted 4 February 2014)

ABSTRACT–Occupant protection of vehicle cab is required for all the commercial vehicles. According to ECE R29-03 amendments, the simulation methods of the front pillar impact test and the side 20° pendulum impact of the roof strength test for a light truck with a gross mass not exceeding 7.5t are proposed. In this study, a reliable finite element model of a light truck is built by using its CAD model. The finite element model is verified against cab modal test and frontal impact test. Then two crash tests are simulated to evaluate the survival space by examining the contact between the deformed cab and a prescribed manikin model. In the front pillar impact test, the deformed cab is predicted to contact with the manikin. In the roof strength test, the minimum distance between the deformed cab and the manikin is predicted to be 75.3 mm, which does not satisfy requirements either. To enhance the crashworthiness of the truck, some structural improvements are designed such as filling structural foam in the A-pillars and the side panels, adding a roof crossbeam, and reinforcing the rear wall of cab. The simulation results of the improved cab structure show that the cab stiffness is improved, the energy absorption is more homogeneous and there is no penetration into the survival space.

KEY WORDS : Crashworthiness, ECE R29, Commercial vehicle, FEA, Occupant safety, Vehicle design

1. INTRODUCTION

The legal requirement for the occupant safety is described in ECE R29-03 standard which is already in force in Europe. A front pillar impact test (Test B) and side 20° pendulum impact test (Test C) for the category N2 and N3 vehicles each with a weight greater than 7.5t were added at the ECE R29-03 amendments. Test B and C setup are shown in Figure 1 and Figure 2.

The front pillar impact (Test B) test examines the strength of A-pillar in the event that a vehicle rolls over 90° and hits trees or cylindrical objects. The side 20° pendulum impact test (Test C) of the roof strength test examines the strengths of the side panel and the roof in the situation that a vehicle rolls over 180° and hits the ground.

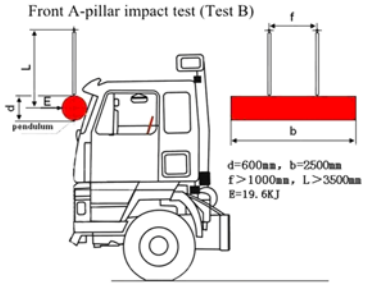

Figure 1. Front A-pillar impact test (Test B).

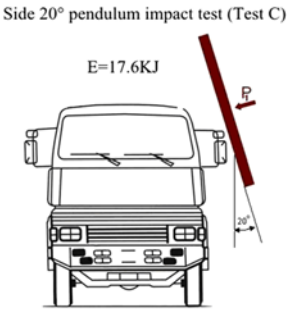

Figure 2. Side 20° pendulum impact test (Test C).

To investigate the vehicle crash behaviors, vehicle tests at various impact conditions have been conducted for a long history. As the cost-effective alternatives to real vehicle tests, finite element analysis (FEA) or simulations of vehicle impact events and the crash tests have been widely adopted in the recent decades because simulation results allow vehicle designers to predict vehicle behaviors,

*Corresponding author. e-mail: liangmo@mail.njust.edu.cn

draw important conclusions, therefore to optimize the structural design at a very early stage of vehicle development process.

A number of automotive engineering researches have been conducted to evaluate vehicle safety according to ECE R-29 regulation. Gendar (2007) applied the explicit finite element method to predict the deformation of driver cabins and presented an example of one of the cabins. The simulation result was compared to the results from the physical test carried out as per ECE R-29 regulation. Tonioli *et al*. (2000) adapted a durability finite element model into a crashworthiness model and performed simulations in LS-DYNA® 3D for various testing conditions according to the ECE R-29 standard. Patidar *et al*. (2005) discussed the practical problems occurred during the implementation of the ECE R-29 standard in Indian and suggested the possible solutions. de Castro *et al*. (2001) addressed the structural assessment of a heavy truck cabin with respect to the occupant response in the designed test of frontal collision according to ECE R-29. Wang *et al*. (2010) comparatively analyzed the inconformity between the frontal pendulum impact test and 180° top cover quasi-static pressure test based on the current ECE R29-02, which is essentially adopted in China for a vehicle collision. The discrepancy between the prevailing ECE R29-02 and ECE R29-03 was interpreted; later on, Wang *et al*. (2011) also improved some design aspects of a commercial vehicle according to the following damage criterions: cab front suspension brackets were broken; steering column and wheel was removed upward and rearward; cab was deformed seriously. Li *et al*. (2005) introduced the testing methods and requirements of commercial vehicle cabs according to the ECE R29 standard, and further developed a front impact test facility for commercial vehicle cabs.

There have been several attempts to optimize the crashworthiness of vehicle structure by means of new materials and new designs. Sun *et al*. (2013) verified the feasibility of using warm forming aluminum alloy parts to improve the energy absorbing performance of vehicle in crash. They compared the difference among using warm forming aluminum alloy, mild aluminum alloy, and mild steel as the material of the front body parts in the frontal impact simulation of a light car. Bae and Huh (2012) performed thickness optimization of center pillar assembly using a response surface methodology. The crashworthiness of optimum designs with conventional steel and advanced high-strength steel were compared using the full vehicle analysis. Xu *et al*. (2011) compared the energy absorbing abilities of high-performance nanoporous energy absorption system (NEAS) interlayer and polyvinyl butyral interlayer for windshield by conducting the simulations of windshield and pedestrian head impact. They concluded that NEAS interlayer may absorb more energy than PVB interlayer.

Now, a Chinese national compulsive standard, "The protection of the occupant of the cab of a commercial vehicle" (GB26512-2011), has taken its action since January 1, 2012. This regulation is developed via the ECE R29-02 standard. Therefore, based on the ECE R29-03 amendments, we develop the simulation methods of the front pillar impact test and the side 20° pendulum impact of roof strength test for a light truck which has been widely used in China. To verify and improve the crashworthiness of this truck, a reliable finite element model of the truck is built by Hypermesh® and Hypercrash®. The crash tests are simulated by the commercial finite element solver RADIOSS®. The occupant survival space is estimated by examining the distance between the deformed cab and a 50th percentile male manikin model. Then, we improve the structural design of the cab and run the simulations of the two impact tests again. The improved design is proved to enhance the crashworthiness of the light truck. The survival space turns to be enough to protect occupant. The modeling and simulation methods along with the design methodology of this study can be used for evaluating and improving the crashworthiness of similar light trucks to satisfy the ECE R29-03 amendments.

2. FINITE ELEMENT MODEL

By using Hypermesh® and Hypercrash®, a light truck finite element model is established to simulate the cabin safety test procedure described by the ECE R29-03 standard.

2.1. Finite Element Mesh

The meshing software, BatchMesher®, is used to batch mesh the cab by setting fine grid standards. The basic mesh size of the mesh is 10 mm. The quadrilateral elements are adopted with priority for the major structure, while allowing the existence of triangular elements to mesh very complex geometries. After batch meshing, Hypermesh® is used to adjust the meshes at some areas to enhance the quality of the whole mesh.

The light truck cab contains many large area sheet metal parts, connected by welding spots, rivet, and bolt. The main connection type of the cab is welding spot. The spring-beam (Spring Type 13) element is used to model the welding spot by setting the elastic stiffness of six directions and a single tensile failure mode. The failure model is that once the tensile strain reached failure value (0.75), the spring-beam element will be deleted. The final cab model contains 3756 welding spots. The rivets and bolts are modeled by the 1-D rigid elements. The suspension systems are modeled by beam elements with the corresponding cross-section setting. The spring elements are used to connect the cab and the frame. In order to avoid computational instability, the tires are modeled as rigid shell elements. The windshield is modeled by shell elements which are glued to the vehicle body. The hexahedral solid elements are used to model the glue which connects the front windshield and the cab. The elastic modulus, density, and Poisson's ratio of glue material are 50 Mpa, 1.16×10^{-6} kg/mm^3, 0.45, respectively. The whole vehicle model

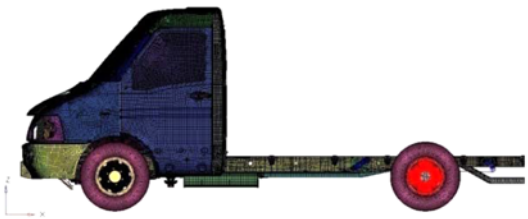

Figure 3. Finite element model of the light truck.

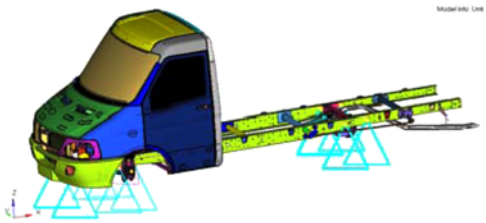

Figure 5. Boundary condition of simulation.

contains 577,168 elements. The cab contains 395,464 elements. There are 537,348 quadrilateral elements and 17,115 triangular elements with a proportion of 2.9%. The finite element model of the whole truck is shown in Figure 3.

2.2. Material and Properties

Vehicle crash process contains large deformations, large strains, and plastic deformations, so the elasto-plastic material models are used in the crash simulations. In RADIOSS, LAW 36 elastic plastic piecewise linear material (M36_PLAS_TAB) is chosen for sheet metals of DC03 material. The elastic modulus, density, Poisson's ratio are set for the linear elastic part, while the stress-strain curves in high-speed tensile tests in different strain rates are set for the non-linear part(Wang *et al*., 2012). For the linear elastic part, the material parameters are summarized in Table 1. The non-linear stress-strain curves of DC03 material are shown in Figure 4.

For the windshield, LAW 27 elastic plastic brittle material (M27_PLAS_BRIT) is used. The failure plastic strain is set to 0.1% to simulate glasses cracking during the test (Sun *et al*., 2005).

For the vehicle model, the shell element type is the reduced integration element QEPH which has an independent normal vector at each node and has one Gauss integration point. According to the RADIOSS theory manual (Altair Engineering, Inc., 2011), QEPH uses physical stabilization hourglass control method so its hourglass performance is better than that of the classic BT element. The calculation accuracy of QEPH is close to the fully integrated element QBAT, while the calculation scale is increased only 15% as compared to the BT element. Hence, the QEPH is chosen for the vehicle crash simulations in this study.

Table 1. DC03 mechanical parameters of the linear part.

Elastic modulus(Gpa)	Density(kg/mm^3)	Poisson's ratio
210	7.89×10^{-6}	0.3

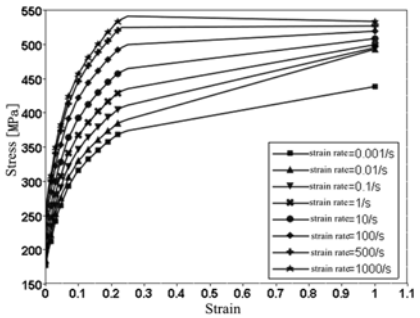

Figure 4. Stress-strain curves of DC03.

2.3. Contact and Boundary Conditions

The general purpose interface (Interface type 7) and edge to edge interface (Interface type 11) are mainly used in the impact simulations. Both of them use the penalty method, but the stiffness is not constant, instead, it increases nonlinearly in order to control the penetration and the negative volume problem in the impact process. In order to control the calculation scale, a variable gap is employed with the range of 0.7~0.8 mm.

According to the ECE R29-03constraint standard, all the degrees of freedom (DOF) of the corresponding points on the frame are fixed (Figure 5).

2.4. Stamping Initialization

Including manufacture effect in finite element vehicle models has been adopted by automotive engineers. Sato *et al*. (2002) carried out the FEA simulations using the material models with both strain rate sensitivity and metal forming effects to evaluate the accuracy of crashworthiness. To improve the accuracy of the crash simulation, one-step stamping initialization was applied to the model in this study. The thickness variation and plastic strain of the cab due to the manufacturing are contained in model at the

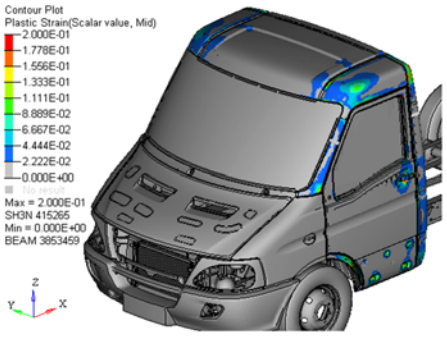

Figure 6. Plastic strain at the initial time.

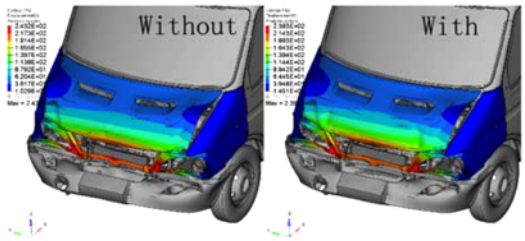

Figure 7. Deformation with or without manufacturing information.

initial time of the crash simulations (Figure 6).

Taking the frontal impact simulations as example, the frontal deformation of the light truck model without manufacturing information is 243.2 mm while the one with the information is 239.3 mm at 50 ms (Figure 7).

3. MODEL VERIFICATION

3.1. Front Impact Test

According to the China mandatory standard, "The protection of the occupants in the event of a frontal collision for motor vehicle" (GB 11551-2003), the 50 km/h frontal impact test of the truck has been carried out as shown in Figure 8. After collision, the seat belt didn't loose and no fuel leaked. The door didn't open during the collision process, and it was opened smoothly without any tool after the test.

The finite element model of the light truck is verified against the frontal impact simulation by using RADIOSS®. The trial truck's cab weight is 1935 kg. The collision speed and angle are 50 km/h and 0°, respectively. A lumped mass is used to simulate the rear cargo box.

As shown in Figure 9, the deformations of the hood and fender in simulation match the test results. Again, as shown in Figure 9, the windscreen does not break; the deformation of the door is small. Hence the living space is sufficient.

The finite element model of the vehicle is partially validated by the comparison between the deformed shapes of the test and the front impact simulation.

3.2. Modal Test

To further verify the accuracy of the established cab

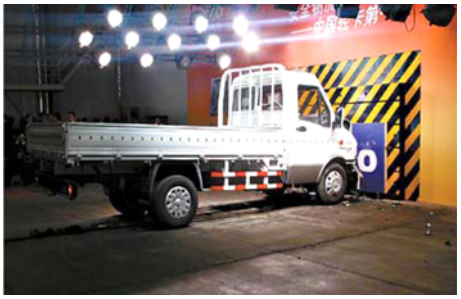

Figure 8. Frontal impact test.

Figure 9. Comparison of real test and simulation results.

Table 2. Comparison of modal test and simulation.

Modal order	Test results (Hz)	Simulation results (Hz)	Errors (%)
1	24.85	23.27	6.36
2	28.46	28.83	1.30
3	32.91	34.54	4.95
4	36.00	38.11	5.86
5	41.60	43.33	4.16
6	46.25	46.98	1.58

models, the BIW modal test and simulation were carried out. According to the BIW modal test requirements, fenders, engine hood, headlight bracket and windshield were removed. For the modeling of welding spots, elastic-plastic beam elements are replaced by solid elements. The cab modal analysis model contains 307031 elements and weights 164.8 kg/h.

Comparing the test results with the simulation counterparts in terms of modal frequencies, as shown in Table 2, both have good consistency. Hence, the developed simulation platform serves a valuable guide to the real vehicle crash tests.

4. CRASH SIMULATIONS BASED ON ECE R29 STANDARD

4.1. Simulation Setup

In ECE R29-03, the front pillar impact test and side 20° pendulum impact of roof strength test is only set for the vehicle with a gross vehicle mass exceeding 7.5t. The original impact energy of front pillar impact test is 29.4kJ, side 20° pendulum impact energy is 17.6kJ. The light truck in this study is 1935 kg. In order to have a more comprehensive examination on the crashworthiness of the light truck, low energy front pillar impact test and side 20° pendulum impact test are carried out.

Referring to front impact (Test A) in the ECE R29-03 standard, the impact energies are 29.4kJ and 55K for vehicles not exceeding 7.5t and exceeding 7.5t, respectively, therefore, the energy ratio is 0.53 (29.4kJ to 55kJ). The ratio is 0.67 in ECE R29-02 standard. For a more stringent test of the light truck, the 0.67 is chosen to determine impact energy. Hence, the new front pillar impact energy is set to 19.6kJ. Simultaneously, the new Side 20° pendulum impact energy is set to 11.7kJ.

The pendulum in test B weighs 1000 kg. Its diameter and length are 600 mm and 2500 mm, respectively. The center of mass of the pendulum is at the midpoint of the front windshield in Z direction and its suspension is longer than 3500 mm. The equivalent angular velocity of the pendulum is 1.787 rad/s and it has the impact energy of 19.6kJ. The impactor in test C weighs 1500 kg, and it is sufficiently large to cover the side panel. The angle between the impactor and the side panel is 20°.

4.2. Survival Space Estimation

The survival space is estimated by using a manikin (Figure 10) built in CATIA®. The manikin model is imported into the final deformed truck model in Hypermesh®. The manikin "H" point coincides with the seat "R" point, when the seat is adjusted to the middle position. In a satisfactory survival space, the manikin does not contact with any non-resilient part of the cab. In addition, the cab should stay connected with the frame even if the connecting parts are expected to be deformed or damaged. At the same time, the door does not open in test process and can be opened smoothly without using any tools after impact test.

4.3. Front Pillar Impact Test

Test B simulation is carried out by RADIOSS® solver (10.0.5 version) with a constant time step set to 5×10^{-7}s. The vehicle mass variation is 1.16%. The deformation and energy change of the front pillar impact test are shown in Figure 11. The living space is shown in Figure 12.

As shown in Figure 11, at 162 ms, the internal energy achieves maximum. The contact energy is the friction energy transferred from the kinetic energies of contacted parts. The maximum dynamic deformation of the cab is 307.3 mm. At 240 ms, when the impact finished, the plastic deformation is 260.1 mm. Therefore, it is more reasonable to estimate the minimum living space during collision rather than after collision to ensure the safety of the occupant.

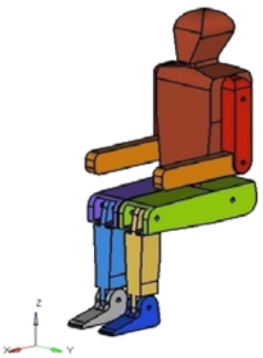

Figure 10. Fifty percentile male manikin model.

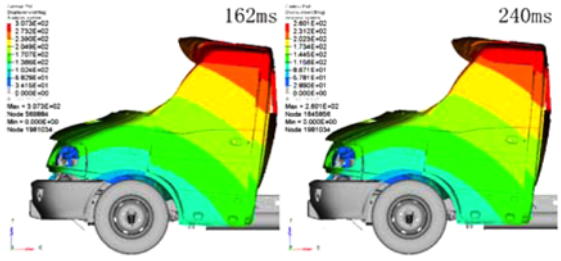

(a) Deformation

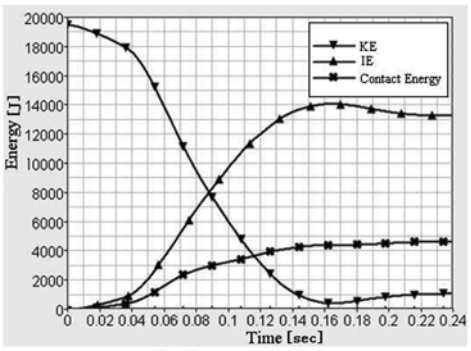

(b) Energy change

Figure 11. Front pillar impact test.

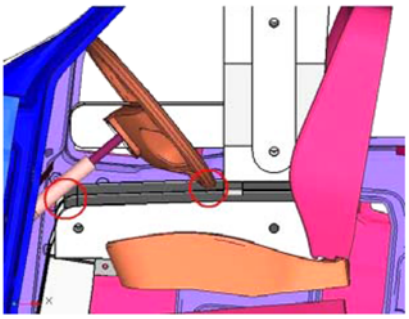

Figure 12. Contact between the manikin and cab.

As shown in Figure 12, using the simulation result at 162 ms, there are contacts between the manikin leg and steering wheel, and the knee and steering column. So the survival space of the truck doesn't meet the requirements and needs to be improved.

4.4. Side 20° Pendulum Impact Test

The constant time step of Test C is the same as Test B, the vehicle mass variation is 0.41%. As shown in Figure 13 (a), at 158 ms, the maximum dynamic deformation of cab is 381.2 mm. At 300 ms, when the impact finished, the plastic deformation is 319.2 mm. The deformation and energy change of the side 20° pendulum impact test is

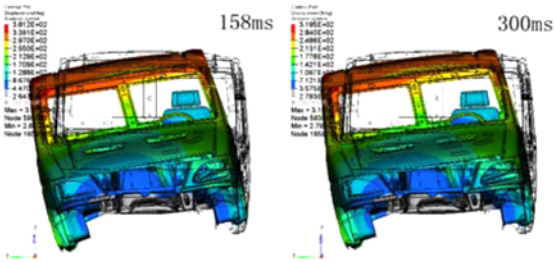

(a) Deformation

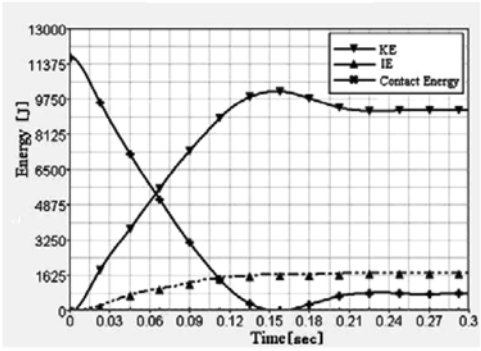

(b) Energy change

Figure 13. Side 20° impact test.

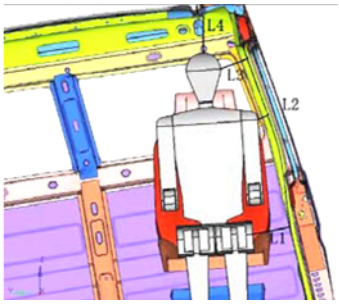

Figure 14. Survival space check of side impact test.

shown in Figure 13 (b).

At 158 ms, as shown in Figure 14, the distance L1 between the manikin knee and the side panel is 189.4 mm; the distance L2 between the shoulder and the side panel is 75.3 mm; the distance L3 between the head and the side panel is 162.6 mm; and the distance L4 between the head and the roof is 174.8 mm. In the initial state, L1, L2, L3, and L4 are 283.5 mm, 239.7 mm, 368.9 mm, and 230.4 mm, respectively. The living space of the truck is small, so it needs to be improved.

5. IMPROVEMENT OF CAB STRUCTURE

Some design improvements on the cabin are carried out to increase the crashworthiness of the light truck by referring to some published works to enhance the vehicle crashworthiness (Cao *et al*., 2009; Pathare and Mansour, 2009).

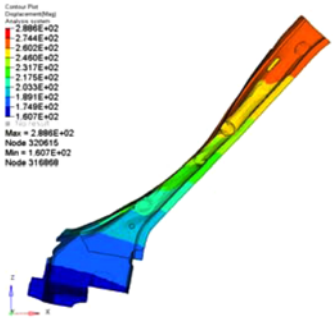

Figure 15. Deformation of the A-pillar.

5.1. Structure Improvement for Front Pillar Impact Test

By observing the deformation of the various parts of the cab, it can be found that there are three parts need to be improved. The first one is the A-pillar, which directly contacts with the pendulum. As shown in Figure 15, at 162 ms, A-pillar is serious collapsed, the maximum dynamic deformation in X direction is 288.9 mm in the middle of the A-pillars. A-pillar can't transfer impact forces to the rear wall and the floor effectively once collapsed.

As shown in Figure 16, the structure foam is inserted in the middle of A-pillar which contacts with the pendulum in order to improve crashworthiness. The foam material is BateFoam 87100/87124 (Dwivedi *et al*., 2011). The

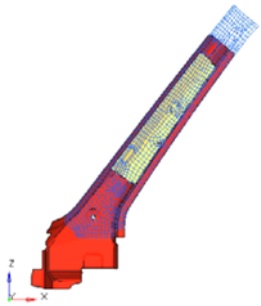

Figure 16. A-pillar structure foam enhancement.

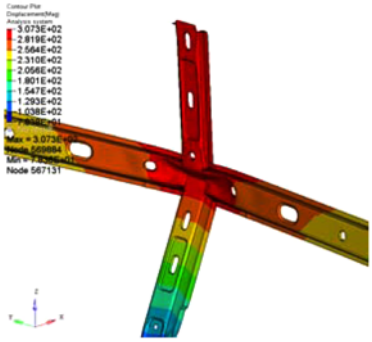

Figure 17. Deformation of the rear wall horizontal beam and the longitudinal beam.

compression modulus, density, Poisson's ratio are 85Mpa, 384 kg/m^3, 0.35, respectively.

The second part needs to be improved is the rear wall horizontal beam which has the 307.3 mm maximum dynamic deformation in X direction and was crushed, as shown in Figure 17, but at the same time the longitudinal beam is not crushed, implying that the stiffness allocation of the two beams is mismatched. Since the horizontal beam is crushed much earlier than the longitudinal beam, the ability of the longitudinal beam to absorb energy is not fully used.

A reinforcing plate was added in the horizontal beam covering the serious deformed part (Figure 18). The material type of the reinforcing plate is HSA340. The non-linear part stress-strain curve of HSA340 is shown in Figure 19.

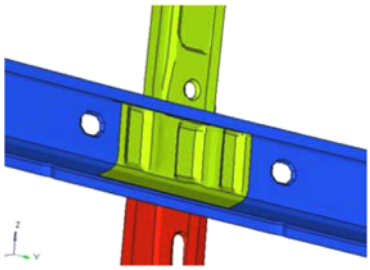

Figure 18. Reinforcing plate in the horizontal beam.

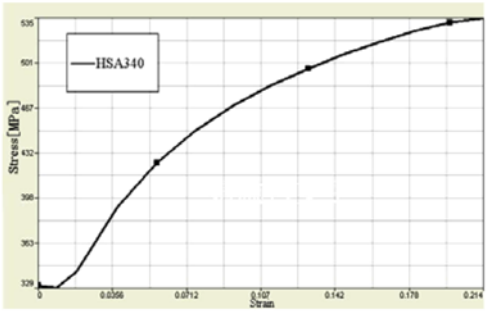

Figure 19. Stress-strain curve of HSA340.

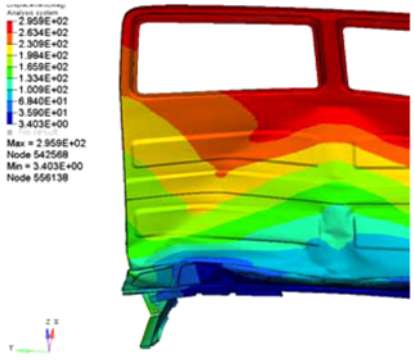

Figure 20. Deformation of the rear wall and the floor.

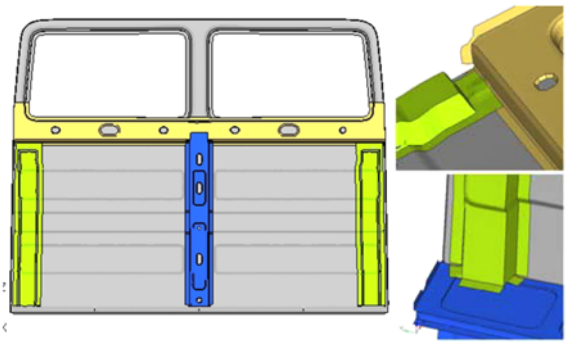

Figure 21. Rear wall longitudinal beam enhancement.

The third part needs to be improved is the connecting part between the B-pillar and the floor beams. Its collapse initiates an inhomogeneous distribution of deformation on the rear wall, therefore inducing the 295.9 mm maximum dynamic deformation of the real wall in X direction (Figure 20).

Two longitudinal beams made of material HSA340 for the rear wall are added to increase the bending stiffness of the rear wall (Figure 21).

5.2. Structure Improvement for Side 20^o Pendulum Impact Test

There are two parts need to be improved in the side 20^o pendulum impact test.

The first part is the top of the left side panel, as shown in Figure 22, at 16 ms the panel is serious collapsed with the

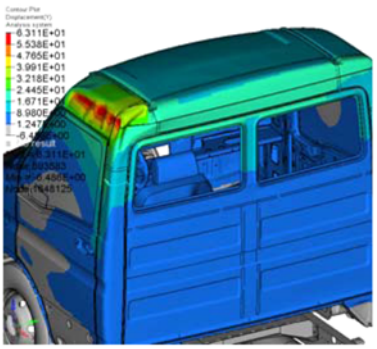

Figure 22. Deformation of the left side panel.

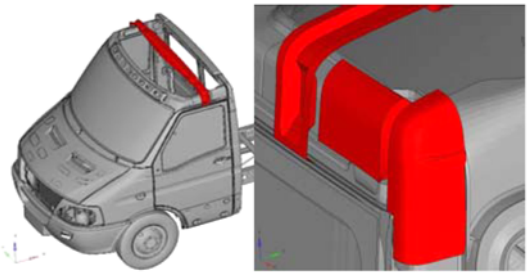

Figure 23. Crossbeam and structure foam enhancement.

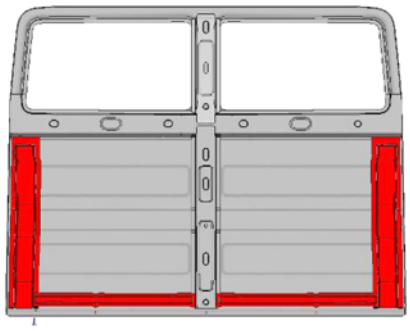

Figure 24. Rear wall horizontal beam enhancement.

63.1 mm maximum Y direction dynamic deformation. But the maximum Y direction deformation of the right side panel only 16 mm at same time. In addition, since there is a large gap between the inner and outer panels of the side panels, the inner panel does not absorb enough energy when the outer panel is already crushed.

As shown in Figure 23, a roof crossbeam is added to transfer the forces from the impacted side panel to the other side panel. The material of crossbeam is HAS340. The structure foam is inserted in side panel between the inner and outer panels to help the inner panel absorb impact energy.

The second part needs to be improved is the bottom of rear wall with 294.2 mm maximum Y direction dynamic deformation. Two horizontal beams are added to the bottom of rear wall, connecting with the longitudinal beams to constitute a complete closed frame, as shown in Figure 24.

5.3. Results of Improved Structure in Front Pillar Impact Test

As shown in Figure 25, the internal energy of the improved truck achieves maximum at 153 ms, a 9 ms reduction compared to the original truck design.

As shown in Figure 26, the deformation of the improved truck was 259.2 mm, a 48.1 mm reduction compared to the original truck.

As shown in Figure 27, the improved A-pillar remains

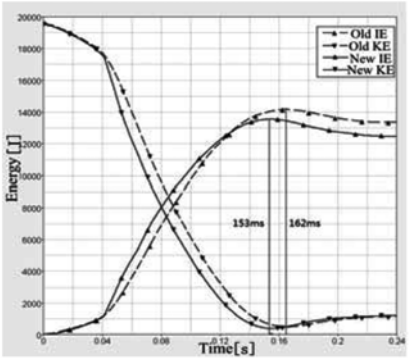

Figure 25. Energy change before and after improvement.

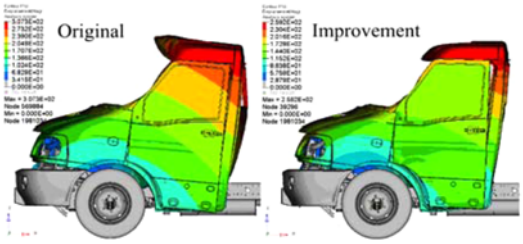

Figure 26. Deformation before and after improvement.

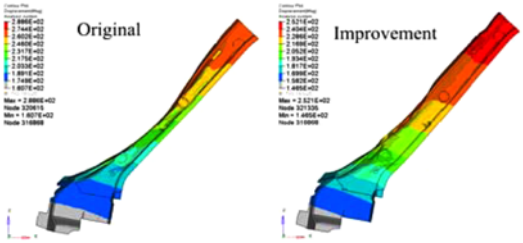

Figure 27. Pillar deformation before and after improvement.

intact and is not crushed. The maximum deformation of the improved A-pillar is 252.1 mm, a 36.5 mm reduction compared to the original one. Therefore it can effectively transfer the impact forces to the rear wall and the floor though the roof.

The maximum deformation of the improved horizontal beam is 278.5 mm, a 28.8 mm reduction compared to the original one. The deformation of the connecting part between the B-pillar and floor beams is 249.4 mm, a 46.5 mm reduction compared to the original one.

As shown in Table 3, the A-pillar absorbs 1.06% more energy after being improved, and the reinforcing plates absorb 0.66% energy. The floor, rear wall, 1st roof beam and roof absorb less energy than the original designs do, but the maximum deformation of the improved truck is less than that of the original design, indicating that more components contribute to the energy absorption.

The Energy absorption ratios of the roof and 1st roof

Table 3. Energy absorption ratio of the parts.

Components	Original	Improvement	Difference
Floor	19.98%	19.47%	-0.51%
A-pillar	16.32%	17.38%	+1.06%
Rear wall	10.09%	8.53%	-1.56%
B-pillar	5.46%	5.67%	+0.19%
1st roof beam	4.34%	1.93%	-2.41%
Roof	3.18%	1.05%	-2.13%
Reinforcing plates		0.66%	

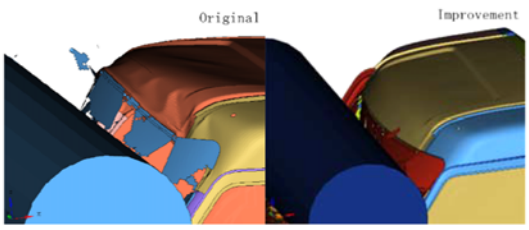

Figure 28. Roof deformation before and after improvement.

beam are less than that of the original design of the truck. Figure 28 shows the deformations of the roof before and after improvement. It is found that the broken windshield is stuck between the pendulum and the roof in the original front pillar impact test. Therefore, the impact force is transferred to the roof directly through the windshield. In the improved front pillar impact test, the force transfer path is changed, thus the energy absorption ratios of the roof and 1st roof beam are reduced.

As shown in Figure 29, the maximum impact force is 58590N, which is 24.24% less than the original design of the truck. Therefore, the structure foam in A-pillars is effective to reduce the impact force.

As shown in Figure 30, at 153 ms, the distance L1 between the manikin body and the steering wheel is 64.3 mm; the distance L2 between the leg and steering wheel is 12.3 mm; and the distance L3 between the knee and the steering column is 28.9 mm. The survival space of the improved truck design in the test B meets the requirements of ECE R29-03 standard.

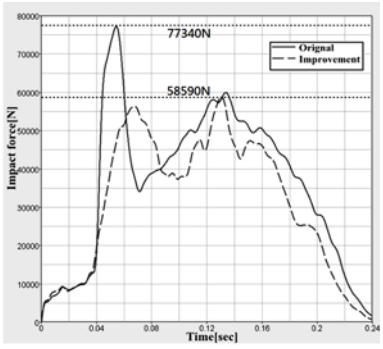

Figure 29. Impact force before and after improvement.

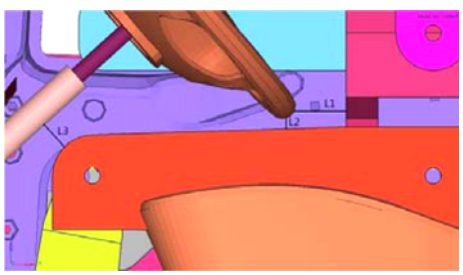

Figure 30. Survival space check of front pillar impact.

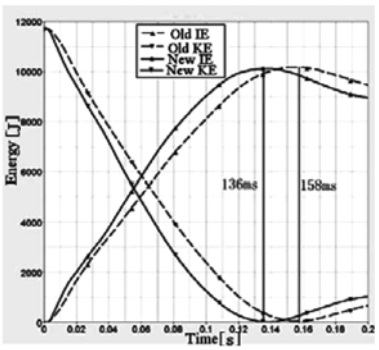

Figure 31. Energy change before and after improvement.

5.4. Results of Improved Structure in Side 20° Pendulum Impact Test

As shown in Figure 31, the internal energy of the improved truck achieves maximum at 136 ms a 22 ms reduction compared to the original truck. From 0 to 11ms, the internal energy of the improved truck increases faster than the original truck, indicating the presence of structural foam and the roof crossbeam enhance the energy absorption speed of the side panels.

As shown in Figure 32, the maximum deformation of the improved truck is 320.1 mm a 61.1 mm reduction compared to the original truck.

As shown in Figure 33, the roof deformation of the improved truck is smaller than the original one, and the distribution is more homogeneous.

The deformation of the rear wall is 276.7 mm, a 17.5 mm reduction compared to the original one (Figure 34).

As shown in Table 4, although the firewall, B-pillar and

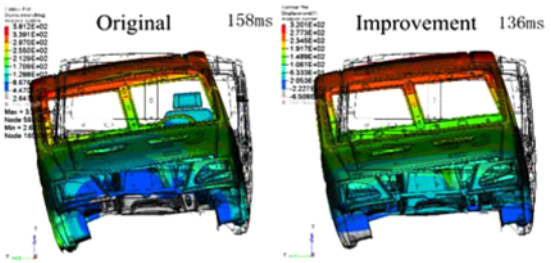

Figure 32. Deformation before and after improvement.

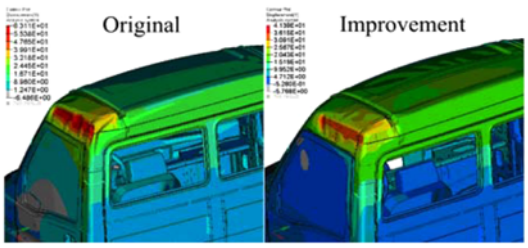

Figure 33. Side panel deformation before and after improvement.

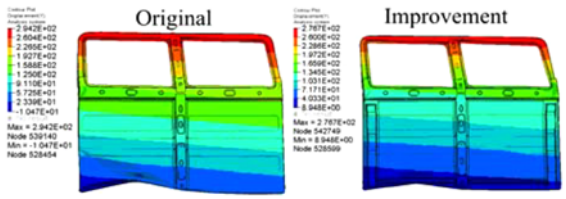

Figure 34. Rear wall deformation before and after improvement.

Table 4. Energy absorption ratio of the parts.

Components	Original	Improvement	Difference
Firewall	24.15%	20.00%	-4.15%
Floor beam	15.12%	15.71%	+0.59%
Rear wall	8.16%	13.33%	+5.17%
B-pillar	13.05%	10.17%	-2.88%
Rear wall beam	1.75%	3.15%	+1.40%
Roof	5.78%	2.93%	-2.85%
Inner side panel	2.78%	1.68%	-1.10%
Reinforcing plates		4.46%	

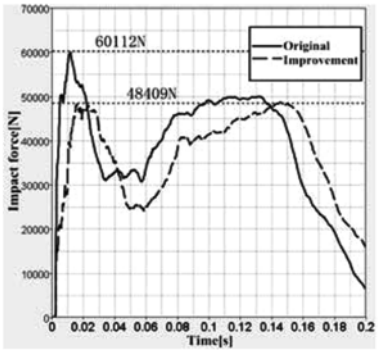

Figure 35. Impact force before and after improvement.

roof absorb less energy than before, but the rear wall and the cross beam absorbs 6.57% more energy after being improved, and the reinforcing plates absorb 4.46% energy.

As shown in Figure 35, after the improvement, the maximum impact force is 48409N, which is 19.47% less than that of the original design.

At 136 ms, the minimum distance of L2 between the manikin shoulder and the side panel is 121.9 mm (not shown here), a 46.6 mm increase compared to the original one. The living space of the improved light truck design is satisfactory for occupant safety.

6. CONCLUSION

This paper carries out simulations for two testing conditions based on the ECE R29-03 amendments. A truck crashworthiness finite element model is built by Hypermesh® and Hypercrash®, and is used for the simulations in RADIOSS. A manikin model is inserted in the deformed cab model to estimate the survival space. The conclusions are as following:

(1) By comparing the modal test results with the simulation ones in terms of modal frequencies, and by comparing the frontal deformation of the front impact test and the simulation one, the finite element model of the truck is partially validated. The modeling method for the light truck is useful for the future crashworthiness modeling of light trucks.

(2) The ECE R29-03 standard criterion for acceptance only deals with the living space after the collision. However, in the collision process, the steering wheel and steering column may have invaded the living space and rebounded to a non-invade position in the final status. Our method to estimate living space uses the truck status at the time when the deformation of the cab reaches maximum. It is a kind of benefit of simulation to observe the minimum living space during impact.

(3) According to ECE R29-03 amendments, simulation methods of front pillar impact test and side 20° pendulum impact of roof strength test for a light truck with a gross vehicle mass not exceeding 7.5t are introduced. The simulations show that the cab is crushed. By using a 50th percentile male manikin, it is estimated that the living space does not meet the requirements in front pillar impact test, and that the minimum living space in the side 20° pendulum impact test is 75.3 mm, which is not satisfactory. The proposed manikin to estimate the vehicle survival space is useful for the front pillar impact test and roof strength test of light trucks.

(4) To enhance the crashworthiness of the light truck, some improvement in structure design are proposed such as filling structural foam in the A-pillar and the side panels, adding a roof crossbeam, and adding reinforcing beams on the real wall of the cab. The simulation results showed that the cab stiffness is improved, the energy absorption is more homogeneous, and there is no penetration into the survival space. Therefore, the structure design improvement of the light truck works.

Future improvement in the modeling of welding spots for the finite element truck model has been planned. There are a number of published failure models for welding spots. Ha *et al*. (2013) proposed a new equivalent failure strength model for welding spot of advanced high-strength steel to describe the failure behavior of welding spots in the crash analysis or strength analysis of a vehicle body. Nguyen *et al*. (2012) revealed that different failure modes of welded parts can be predicted and simulated using the EWK rupture model available in the PAM-CRASH commercial CAE tool, in which the proposed models and analyses can be used for simulations of crashworthiness. We will compare these available failure models of welding spot and

implement the most suitable failure model in the Radioss software for crashworthiness simulations.

ACKNOWLEDGEMENT–The author would like to acknowledge the support of Prospective Study Project of Production, Studying and Researching of Nanjing, Jiangsu Province, China (2013ti122115) and Prospective Study Project of Production, Studying and Researching of Jiangsu Province, China (BY2009109).

REFERENCES

Altair Engineering, Inc. (2011). RADIOSS Theory Manual 11.0 Version. Altair Engineering, Inc.

Bae, G. H. and Huh, H. (2012). Comparison of the optimum designs of center pillar assembly of an auto-body between conventional steel and ahss with a simplified side impact analysis. *Int. J. Automotive Technology* **13**, **2**, 205–213.

Cao, L., Bai, Z., Wu, J., Cui, C. and Niu, Z. (2009). Structural improvement for the crash safety of commercial vehicle. *SAE Paper No.* 2009-01-2917.

De Castro, I., Jokuszies, M., Altamore, P. and Lee, W. (2001). Simulation of occupant response in the ECE R29 safety test. *SAE Paper No.* 2001-01-3845.

Dwivedi, P., Kulkarni, A., Chalipat, S. and Pardeshi, M. (2011). Protection devices to improve frontal pendulum impact performance of heavy commercial vehicles. *SAE Paper No.* 2011-26-0099.

ECE R29-03 (2010). Uniform provisions concerning the approval of vehicles with regard to the protection of the occupants of the cab of a commercial vehicle.

GB 11551-2003 (2003). The protection of the occupants in the event of a frontal collision for passenger car.

GB 26512-2011 (2011). The protection of the occupants of the cab of a commercial vehicle.

Gendar, D. (2007). Numerical simulations for testing of commercial vehicle as per ECE-R29 regulations. *SAE Paper No.* 2007-26-045.

Ha, J., Huh, H., Song, J. H. and Lim, J. H. (2013). Prediction of failure characteristics of spot welds of DP and trip steels with an equivalent strength failure model. *Int. J. Automotive Technology* **14**, **1**, 67–78.

Li, S., Guo, K., Zhao, Y. and Guo, Y. (2005). Frontal pendulum impact test and computer simulation of commercial vehicles. *China Mechanical Engineering* **16**, **23**, 2153–2156.

Nguyen, N. T., Kim, D. Y., Song, J. H., Kim, K. H., Lee, I. H. and Kim, H. Y. (2012). Numerical prediction of various failure modes in spotwelded metals. *Int. J. Automotive Technology* **13**, **3**, 459–467.

Pathare, R. and Mansour, M. (2009). Automotive roof crush structural foam enhancement solution. *SAE Paper No.* 2009-01-0371.

Patidar, S., Tandon, V., Mahajan, R. and Raju, S. (2005). Practical problems in implementing commercial vehicle cab occupant protection standard ECE R-29. *SAE Paper No.* 2005-26-041.

Sato, K., Yoshitake, A., Zeng, D. and Liu, S. (2002). Crashworthiness of automotive stamped parts using high strength steel sheets. *SAE Paper No.* 2002-01-0641.

Sun, D. Z., Andrieux, F., Ockewitz, A., Klamser, H. and Hogenmüller, J. (2005). Modelling of the failure behaviour of windscreens and component tests. *LS-DYNA Anwenderforum, Bamber* B-II-23.

Sun, H. T., Wang, J., Shen, G. Z. and Hu, P. (2013). Application of warm forming aluminum alloy parts for automotive body based on impact. *Int. J. Automotive Technology* **14**, **4**, 605–610.

Tonioli, J., Castro, I., Ripoli, R. and Argentino, M. (2000). Computational simulation of the ECE R-29 safety test. *SAE Paper No.* 2000-01-3524.

Wang, D., Liu, L., Su, Y., Guo, L., Zhang, C., Tang, H. and Li, H. (2010). Research and analysis concerning commercial vehicle cab strength test requirements. *Automobile Technology*, **10**, 50–53.

Wang, D., Liu, L., Su, Y., Guo, L., Zhang, C., Tang, H. and Li, H. (2011). A study on the impact safety of commercial vehicle cab and its improvement. *Automotive Engineering* **33**, **1**, 2–5.

Wang, L., Chen, D., Yuan, L., Zhang, Z. and Zhang, T. (2012). Simulation and improvement of safety performances of a certain school bus. *J. Nanjing University of Science and Technology (Nature Science)* **36**, **6**, 1031–1035.

Xu, J., Li, Y. B., Chen, X., Ge, D. Y., Liu, B. H., Zhu, M. Y. and Park, T. H. (2011). Automotive windshield-pedestrian head impact: Energy absorption capability of interlayer material. *Int. J. Automotive Technology* **12**, **5**, 687–695.